

THE EVALUATION OF THE WEAR MECHANISM OF HIGH-CARBON HARDFACING LAYERS

Materials based on cast irons are often used for protection against wear. One of the methods of creating protective surface with cast iron structures is hardfacing. The application of hardfacing with self shielded flux cored wire with high carbon content is one of the economical ways often used to protect machinery parts exposed to both abrasion and erosion. The wear resistance of hardfacings depends on their chemical composition, structure obtained after hardfacing, parameters of depositing process and specific conditions of wear. As the base material in the investigation the steel grade S235JR was used. The wear behavior mechanism of hardfacings made with one type of self shielded flux cored wire and different process parameters were evaluated in this paper. Structures obtained in deposition process were different in hardness, amount of carbides and resistance to wear with two investigated impingement angles. The erosion tests showed that impingement angle 30° gives lower erosion rate than angle 60°.

Keywords: hardfacing, self shielded flux cored arc welding, cast iron, erosion, wear, structure

1. Introduction

There is variety of techniques and materials for increasing hardness and creating protective surface against wear. Using welding techniques it is possible to apply ceramic particles in alloys [1-3] or modify the surface of ceramic by metals [4]. These samples show the wide possibility of applying the hardfacing processes in improving surface properties. Most of the hardfacing techniques are based on the welding processes [5] and high carbon and chromium materials. Thank to their good wear resistance and low cost, iron-based hardfacing alloys are frequently employed in industry to extend the service life of components subjected to abrasive, erosive or metal to metal wear conditions, such as rocking pulverizing, crushing to applications and transport systems [6-13]. One of the interesting hardfacing techniques is self shielding arc welding with cored wire. The construction of the filler material gives possibility of creating deposits with chemical composition typical for the cast iron and enabling high productivity. The good correlation of wear resistance of iron-based hardfacing alloys, with respect to manufacturing cost, primarily depends on the formation of hard M_7C_3 carbides. The problem is that brittle and coarse M_7C_3 chromium carbides tend to separate from the matrix during the wear process, the efficiency of the application of these iron-based hardfacing alloys to parts exposed to heavy external conditions is limited. However, if carbides in the structure of the weld pad are smaller, harder and uniformly distributed, abrasives can not

effectively penetrate into the matrix and carbides are not easily separable from the matrix. In this way wear resistance of iron-based alloy hardfacing under heavy external influences can be improved. Therefore, many researchers are using the addition of strong carbide forming elements such as W, V, Nb, Ti and B [12,14-16]. They are added to the melt in order to obtain other types of carbides for example MC-type, which are smaller and harder than the M_7C_3 carbides. Another way to obtain different size and types of carbides [17-19], or change the geometry of the deposit [20], is the change of the hardfacing techniques and their parameters.

The present research work has the main goal in examinations of microstructure properties on the erosion behaviour of one type of hardfacing alloy that could be applied on chutes in mining industry. The wear behaviour investigations were focused on damage produced by multiparticle impacts to obtain information on associated material removal mechanisms.

2. Experimental procedure

One type of self shielded cored wire was selected and welded on the 10 mm thick plates from steel grade S235JR. Chemical composition of the hardfacing alloy designed as Corthal[®] 61 OA can be seen in Table 1. The welding parameters are given in Table 2. The welding was carried out in flat position with single layer by the use of Lincoln Electric automated welding machine.

* CZESTOCHOWA UNIVERSITY OF TECHNOLOGY, FACULTY OF MECHANICAL ENGINEERING AND COMPUTER SCIENCE, DĄBROWSKIEGO 69, 42-201 CZĘSTOCHOWA, POLAND

** UNIVERSITY OF ŽILINA, DEPARTMENT OF TECHNOLOGICAL ENGINEERING, UNIVERZITNÁ 1, 010 26 ŽILINA, SLOVAKIA

*** CRACOW UNIVERSITY OF TECHNOLOGY, FACULTY OF MECHANICAL ENGINEERING, 24 WARSZAWSKA STR., 31-155 KRAKÓW, POLAND

Corresponding author: mgucwa@spaw.pcz.pl

TABLE 1

Chemical composition of deposited material

Chemical composition of self shielded cored wire wt. %						
C	Mn	Si	Cr	Nb	B	Fe
5.4	0.4	1.3	22	7	1	Balance

TABLE 2

Hardfacing process parameters

Designation of samples	Width of the weld, mm	Speed of hardfacing, mm/s	Power, W	Speed of oscillation, mm/s
S1	45	3.16	10045	46.6
S2	25	3.16	12915	46.6
S3	45	2.16	12915	28.3

To simulate wear condition that can occur in mining industry on the chutes, the wear tests were performed with the use of modified position consisting of chamber with sand blasting machine and system of fastening samples at the predetermined angle. Samples with hardfaced materials with dimensions of 40×50 mm were prepared for tests. Each sample was weighted before the test and after 60 s of testing until parent material was noticed on testing samples. After each exposure the specimens were removed and cleaned with dry compressed air and weighed on digital electronic balance to an accuracy of 0.001 g. Quantitative wear characterization was done by erosion rate, mass loss of the testing specimen during wear testing divided by the mass of erodent particles used in experiment. The particle feed rate was kept constant throughout the erosion studies and was nominally 13 kg min⁻¹ and velocity 12 m s⁻¹. All the erosion experiments were conducted at room temperature. The specimens were mounted directly ahead the nozzle with a stand off distance of 100 mm between the end of the nozzle and the test surface. Inner diameter of the nozzle was 9 mm. The erosion experiments were performed using silica sand particles, at impingement angles of 30° and 60°.

Characterization of microstructure and wear behaviour were done with optical microscope and scanning electron microscope. The specimens used for metallography were prepared by the use of standard metallographic techniques. The polished specimens of high chromium iron hardfacing alloy were subsequently etched with etching reagent (10 g CuCl₂, 10 ml HCl, 80 ml C₂H₅OH). The microstructure of 2 samples, with lowest and highest carbide volume fraction, was examined using Bruker D8 Advance X-ray diffractometer. Diffraction of X-rays was performed using a copper lamp with a characteristic CuK radiation source. The samples were scanned at an angle range from 20° to 120° with the resolution of 0.02° and exposure time of 3 s per step. The next step of investigation was hardness test. Hardness measurements were carried out with a standard Vickers hardness technique HV30 for macroscopic hardness. To determine the hardness of each phase in microstructure, e.g. hard particles and metallic matrix, HV0.01 was used (Table 3).

3. Results and discussion

The structure and properties of obtained welds show significant differences caused by parametric surfacing which directly resulted in the heat input and the rate of discharge. Thus, using all the time the same filler material a great diversity of structure was achieved, which entailed changes in the functional properties of the deposits.

As a result, it was found that the deposit made with the same parameters does not have a uniform structure throughout the cross-section. There are noticeable differences in hardness, the amount, form and size of carbide precipitates.

TABLE 3

Bulk hardness and microhardness of weld hardfacing deposits

Designation of samples	Bulk hardness HV30	Microhardness of matrix HV0,01	Microhardness of carbides HV0,01	Carbide volume fraction CVF, %
S1	787±38	537±160	1515±455	29.7
S2	761±36	452±118	1320±239	32.2
S3	926±10	443±68	1712±184	38.9

The sample S1 has a structure consisting of longitudinal large primary carbides which occur occasionally, and the entire volume of the weld is dominated by primary and finely dispersed eutectic carbides (Fig. 1). In the weld pad S2 primary carbides are mainly in the form of elongated spindle-shaped precipitates, wherein the size decreases from the surface towards the weld line (Fig. 2). At the same time the occurrence of the primary carbides in the form of polygons and numerous minor separation of eutectic carbides can be noticed. The different nature of the structure of the deposit is sample S3 (Fig. 3). The upper part of the structure is dominated by the longitudinal separation of the primary carbides oriented at an angle of approximately straight relative to the surface of the weld. The XRD analysis showed that the structures in the examined samples were very similar. Fig. 4 shows the presence of the primary M₇C₃ and Nb₆C₅ carbides

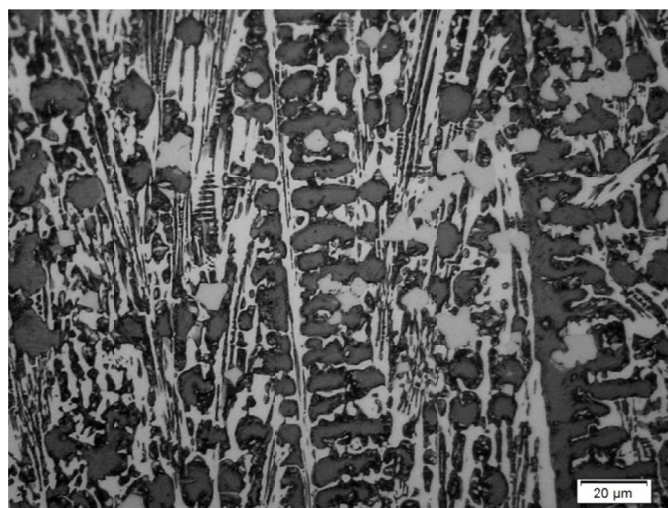


Fig. 1. Microstructure of sample S1

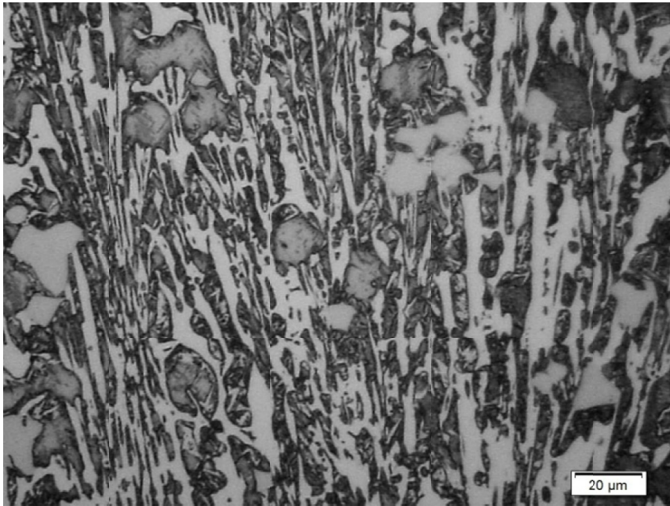


Fig. 2. Microstructure of sample S2

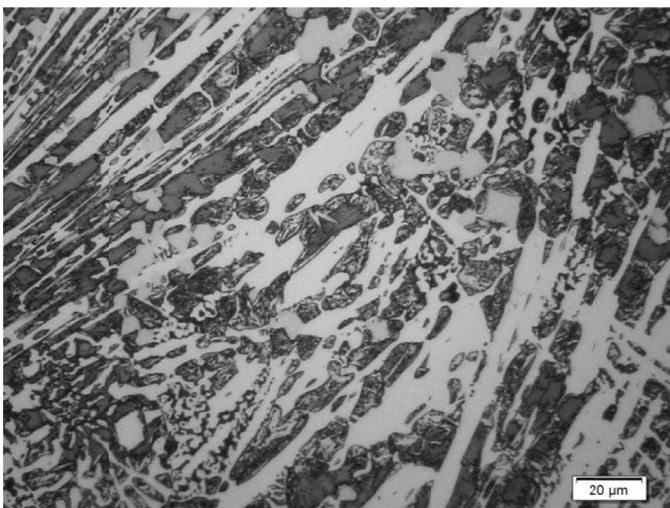


Fig. 3. Microstructure of sample S3

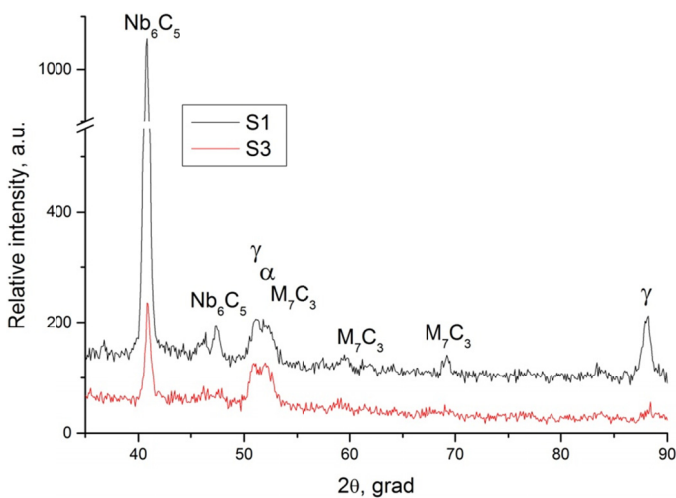


Fig. 4. XRD of deposited samples S1 and S3

in the matrix of comprised of eutectic mixture of austenite and fine M₇C₃ carbides. The spindle shaped primary M₇C₃ carbides (white phase) grow predominantly along the heat flow [17]. The

Nb₆C₅ carbides (gray phase) were observed rather as the hexagonal particles like the most of the M₇C₃ carbides. There were no traces of boron composites in the structure after XRD analysis. This can be attributed to the dominance of the chromium and niobium carbides in the carbides in the structure [21].

The nature of the deposit carbides remain unchanged except for the reduction of such precipitates. In all observed hardfacings shredding the carbides as it approaches the fusion line can be seen. Characteristic fragmentation of the carbides in all the studied welds, which increases with the distance from the surface is caused by a strong heat dissipation into the base metal and dilution of materials [22,23]. The different level of heat input in the hardfacing process invoked fast heat dissipation area of the deposit lying near the line of fusion and caused limited diffusion process as well as prevented the formation of large carbide precipitation [24]. In the above-lying layers of heat dissipation was much slower so the conditions for the diffusion of the alloying elements were much better, and allowed to crystallize large primary carbides, the axes of which are oriented in the direction of heat dissipation.

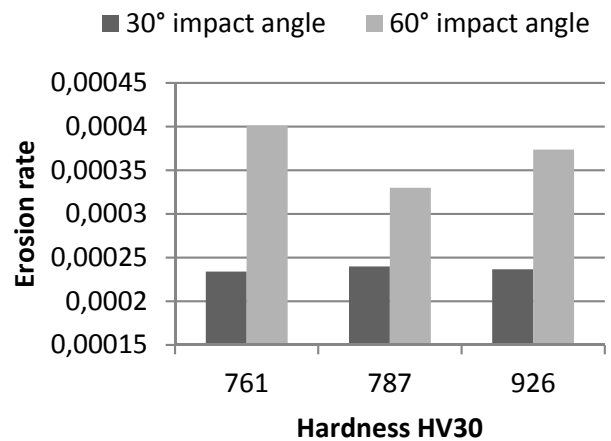


Fig. 5. The comparison of the erosion rate to the bulk hardness of the deposits

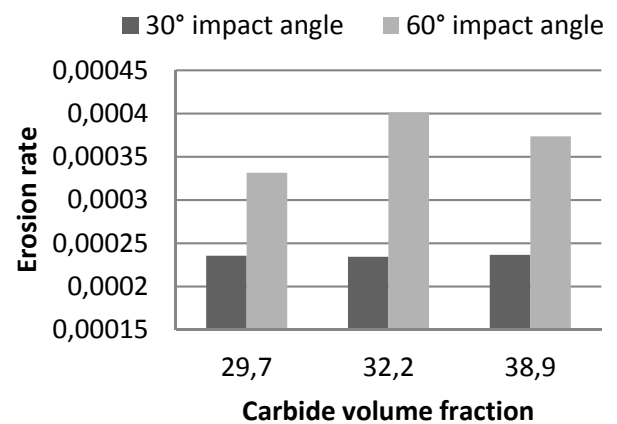


Fig. 6. Erosion rate in relation to the carbides volume fraction

Relationship between impingement angles and erosion rates is shown in Fig. 5. At 60° impingement angle an increasing trend in erosion rate was observed in comparison to the 30°

impingement angle. These results are often observed for the hard materials or coatings, but for the soft materials the results can be reversed [25,26]. The increase in erosion rate was from 40% to 70% bigger than for lower impingement angle. Relative low hardness gives advantages at 30° impingement angle where erosion rate was very close to the whole investigated samples. Fig. 6 shows increasing erosion rate up to carbides volume fraction about 32% and then decrease at 60° impingement angle. There were not observed significant differences in erosion rate depending on the carbide volume fraction at 30° impingement angle.

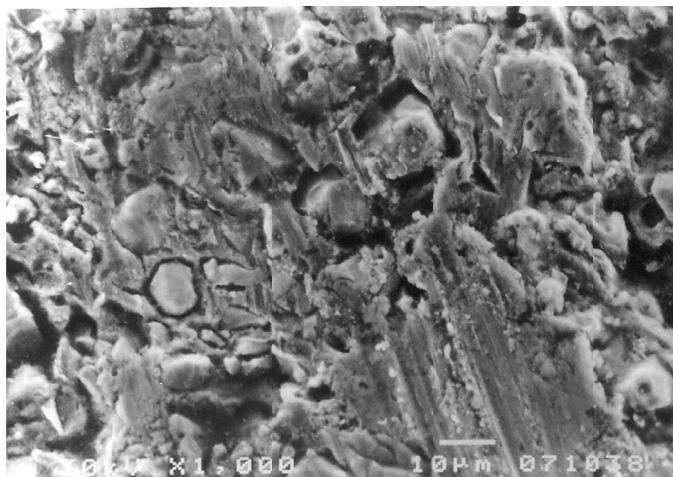


Fig. 7. Traces of erosive particles on sample S3 at 30° impact angle

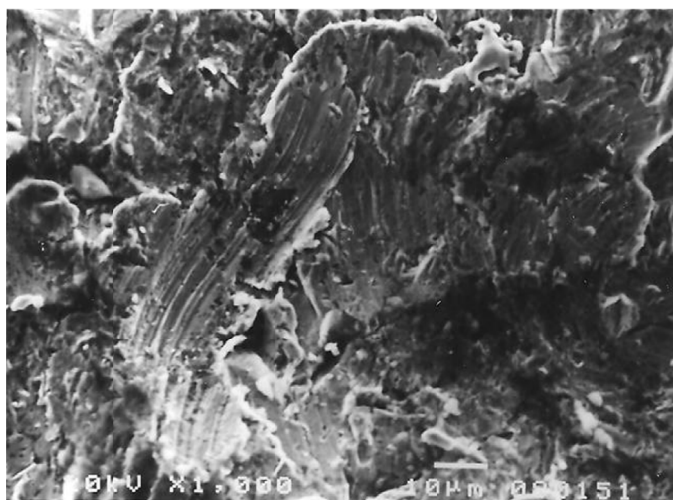


Fig. 8. Traces of erosive particles on sample S1 at 60° impact angle

In Fig. 7 and 8 clear traces of erosive particles were left on the surface of the hardfacing. This is particularly well visible in Fig. 8, which shows that the erosive particle does not move along a straight line. The material is micro-scratched and there are traces of ploughing peeling, splitting off part of the material. Traces of wear that can be observed in these drawings are not arranged in one direction but show some variation caused by changing the direction of incidence of erosive particles. These changes are caused by numerous collisions between erosive

particles. Some of them, after hitting the surface of the hardfacing, were reflected and hitting other particles changed their direction. As a result of erosive action, further parts of material are exposed, as evidenced by the appearance of surface shown in Figure 7. The central part of the drawing shows a fragment of the surface with exposed carbides. It can be seen there the trace after the impact of the erosive particles and the mechanism of carving out the carbides, which are washed away by the abrasive and gradually stripped of matrix around them. In the next step, such weakened carbides are pulled out of the matrix. There is not one factor on which the wear rate depends. There are rather a set of materials properties as for example hardness, structures and carbide volume fraction. In the case of the lower impingement angle the differences in properties of samples do not affect in erosion wear and mechanism of the wear. The situation is different at impingement angle equal 60°. In this condition the erosion rate depends strongly on the properties of the deposit. The sample S1 with hardness close to 800HV30 (Table 3) and lower carbide volume fraction reaches the best level of the erosion rate. Combination of the high hardness of the carbides and their lower contribution in structures allows to minimise the possibility of the cracks of the carbides and strong matrix prevents the carbides from washing out from surface. The high carbide volume fraction works in the opposite way in these conditions. The brittle carbides are very close to each other and this can cause the higher possibility of their cracking due to the lack of the ductile matrix, that could dissipate and absorb the part of the energy of the impact of the erodent particles. The carbides weakly precipitated in matrix are easily separated from the deposited material.

4. Conclusions

- In the experiment a decisive role in the resistance to erosion wear plays the impact angle. At impingement angle 30° there were no significant differences in erosion rate with reference to hardness or carbides volume fraction.
- At impingement angle 60° moderate hardness and low carbides volume fraction gives the best results.
- Main mechanisms of wear in this experiment were scratching and peeling. The crucial point of wear resistant are the carbides implemented in the matrix. The bigger carbides were very easily separated from the matrix and it was the main factor which increased erosion rate.

REFERENCES

- [1] J.I. Iwaszko, K. Kudła, K. Fila, Bull. Pol. Acad. Sci.-Te. **66** (5), 713-719 (2018), DOI: 10.24425/125338.
- [2] J. Górk, A. Czupryński, M. Żuk, M. Adamiak, A. Kopyś, Materials **11**, 1184, (2018), DOI:10.3390/ma11071184
- [3] M. Bonek, Arch. Metall. Mater. **61** (2), 719-724 (2016), DOI: 10.1515/amm-2016-0123.

- [4] T. Chmielewski, D. Golański, W. Włosiński, *Bull. Pol. Acad. Sci.-Te.* **63** (2),449-456 (2015), DOI: 10.1515/bpasts-2015-0051.
- [5] C. Okechukwu, O.A. Dahunsi, P.K. Oke, I.O. Oladele, M. Dauda, *Nigerian Journal of Technology* **36** (4), 1095-1103 (2017), DOI: 10.4314/njt.v36i4.15.
- [6] M. Kirchgaßner, E. Badisch, F. Franek, (2008) *Wear* **265** 772-779 (2008).
- [7] S. Chatterjee, T.K. Pal, *Wear* **261**, 1069-1079 (2006).
- [8] R. Bęczkowski, *Metalurgija* **56**, 59-62 (2016).
- [9] S.G. Sapate, A.V. Rama Rao, *Tribol. Int.* **39**, 206-212 (2006).
- [10] X.H., Tang, R. Chung, C.J. Pang, D.Y. Li, B. Hinckley, K. Dolman, *Wear* **271**, 1426-1431 (2011).
- [11] M.F. Buchely, J.C. Gutierrez, L.M. Le'on, A. Toro, *Wear* **259**, 52-61 (2005).
- [12] J.J. Coronado, H.F. Caicedo, A.L. Gómez, *Tribol. Int.* **42**, 745-749 (2009).
- [13] M. Gucwa, R. Bęczkowski, J. Winczek, T. Wyleciał, *Arch. Foundry Eng.* **17**, 51-54 (2016).
- [14] S. Chatterjee, T.K. Pal, *J. Mat. Process. Technol.* **173**, 61-69 (2006).
- [15] D. Liu, R. Liu, Y. Wei, *Surf. Coat. Technol.* **207**, 579-586 (2012).
- [16] M. Gucwa, J. Winczek, R. Bęczkowski, M. Dośpiał, *Arch. Foundry Eng.* **16**, 39-42 (2016).
- [17] E.O. Correa, N.G. Alcântara, L.C. Valeriano, N.D. Barbedo, R.R. Chaves, *Surf. Coat. Technol.* **276**, 479-484 (2015), DOI: 10.1016/j.surfcoat.2015.06.026
- [18] A. Gualco, H. G. Svoboda, E. S. Surian, *Wear.* **360-361**, 14-20 (2016), DOI: 10.1016/j.wear.2016.04.011.
- [19] N. Yüksel, S. Sahin, *Mater. Des.* **58**, 491-498 (2014), DOI: 10.1016/j.matdes.2014.02.032.
- [20] A. Choudhary, M. Kumar, D.R. Unune, *Defence Technology* **15**, 72-82 (2019), <https://doi.org/10.1016/j.dt.2018.08.004>
- [21] H. Durmuş, N. Çömez, C. Gül, M. Yurddaşkal, M. Yurddaşkal, *Int. J. Refract. Met. H.* **77**, 37-43 (2018), DOI:10.1016/j.ijrm-hm.2018.07.006
- [22] N.G. Chaidemenopoulos, P.P. Psyllaki, E. Pavlidou, G. Vourlias, *Surf. Coat. Technol.* **357**, 651-661 (2019), DOI:10.1016/j.surfcoat.2018.10.061
- [23] S. Pawara, A.K. Jha, G. Mukhopadhyay, *Int. J. Refract. Met. H.* **78**, 288-295 (2019), DOI:10.1016/j.ijrmhm.2018.10.014
- [24] C.M. Chang, C.M. Lin, C.C. Hsieh, J.H. Chen, C.M. Fan, W. Wu, *Mater. Chem. Phys.* **117**, 257-261 (2009), DOI:10.1016/j.matchemphys.2009.05.052
- [25] K.V. Sreenivas Rao, K.G. Girisha K.E. Sushruta, *Mater. Today-Proc.* **4**, 10221-10224 (2016)
- [26] Y. Ben-Ami, A. Uzi, A. Levy, *Powder Technol.* **301**, 1032-1043 (2016), DOI:10.1016/j.powtec.2016.07.041